

The effect of a stepped lip piston design on performance and emissions from a high-speed diesel engine

Felix Leach^{1†}, Riyaz Ismail¹, Martin Davy¹, Adam Weall², Brian Cooper²

1. Department of Engineering Science, University of Oxford, Oxford, UK
2. Powertrain Research and Technology, Jaguar Land Rover Ltd, Coventry, UK

† Corresponding Author: felix.leach@eng.ox.ac.uk

Abstract

Understanding engine-out NO_x and soot emissions from light-duty diesel engines is vital for improving combustion system design and ultimately for reducing aftertreatment requirements. In this work two piston bowl shapes, a standard re-entrant bowl and a bowl with a stepped lip, are tested experimentally and numerically at two part-load operating points (1500 rpm/6.8 bar net IMEP and 1750 rpm/13.5 bar net IMEP), and four full-load operating points (1500, 2000, 3000, and 4000 rpm). The results show that the stepped lip design consistently increases the 50-90 % MFB duration across all operating conditions due to the trapping of the flame in the region of the stepped lip. Use of the stepped bowl allowed injection timing to be advanced at full load, a condition constrained, in this work, by strict limits of cylinder pressure and exhaust temperature. However, despite these changes in combustion behavior engine out emissions were found to be largely insensitive to the bowl shape. No statistical difference in NO_x and soot emissions between the two bowl geometries was observed at part load. A minor penalty in NO_x emissions, statistically significant at ~67 % CI, is reported for the stepped bowl design at some full load points.

Keywords: Stepped Bowl, Diesel Combustion, NO_x, Soot

Introduction

Light duty diesel engines are acknowledged to decrease CO₂ emissions and fuel consumption in comparison to similar gasoline engines, however at the cost of increased engine-out NO_x and soot emissions [1]. Today these emissions can be successfully controlled using aftertreatment. However, the costs of diesel exhaust aftertreatment are notably higher than for gasoline engines [2]. Reducing diesel emissions on an engine-out basis would reduce this aftertreatment burden.

Combustion chamber geometry is known to have a major influence on in-cylinder NO_x and soot formation in diesels; spray targeting — and the interaction of the spray and piston at the lip of the piston bowl—will have a significant influence on local fuel/air ratios in both the squish region and the bowl [3-6] and will affect in-cylinder heat transfer [7, 8]. The geometric detail of the combustion chamber and bowl will also have a similar influence [8-10].

Typically, diesel engines have use omega shaped combustion bowls, promoting fuel-air mixing upon fuel injection. Several studies have shown that, for the same compression ratio, a stepped, or ramped, lip on the piston bowl can reduce soot and CO emissions, as well as improving fuel consumption relative to a conventional re-entrant bowl [7, 11, 12]. These studies, although referring to a stepped-lip piston, actually use geometry which is ramped; this allows part of the fuel spray to be directed up away from the bowl improving air utilisation [13] and EGR tolerance [14]. Recently the Mercedes-Benz OM654 engine was launched with a stepped bowl piston (in this case a definite orthogonal step, rather than a ramped shape), this has reported excellent air utilisation, low particulate emissions and higher efficiency (due to a higher burn rate and in reduced heat loss across the cylinder) [15, 16]. Stepped lip pistons which are ramped, in general, will reduce the heat transfer across the piston due to their lower surface area to volume ratio [7] – this change in surface area to volume ratio need not be there for a true orthogonal step.

The referenced literature suggest that the major effect of such a lip is to increase oxygen availability at the point where the spray is targeted, leading to better fuel/air mixing and more complete combustion. All of these studies report a decrease in combustion duration with a stepped lip due to this improved mixing in the lip region. This decrease in combustion duration, combined with reduced heat transfer will lead to the increases in efficiency and decreases in fuel consumption reported.

In this work we investigate the emissions and performance of a modern light-duty high-speed diesel engine when varying the piston bowl shape between a standard bowl and a stepped lip design back-to-back in order to be able to ascertain exactly the effect of the stepped lip shape (as distinct from ramped lip shapes) is having on the combustion and emissions relative to the standard bowl shape. Multi-dimensional modeling, validated against the experimental data, is used to explain and understand the experimental results.

Experimental Method

Engine

A single cylinder diesel engine with a top-end matching the Jaguar Land Rover AJ200D “Ingenium” engine [17] and a production standard fuel injection system was used in this work. The bottom end of the engine is a Ricardo Hydra. The engine and test cell installation has been fully described in [18]. Key engine specifications of the single-cylinder engine are shown in Table 1.

Table 1: Specifications of the single-cylinder diesel engine

Bore × Stroke	83 × 92.4 mm
Displacement	500 cm ³
Valves per Cylinder	2 intake, 2 exhaust
Compression Ratio	15.4 : 1
Fuel Pressure	400-1800 bar
Injector	Production ‘Ingenium’ engine injector

Piston bowls

Two piston bowl shapes are tested: a conventional re-entrant bowl (as used in the Jaguar Land Rover AJ200D “Ingenium” engine), and a bowl fitted with a novel stepped lip geometry. The stepped lip bowl is designed to be as similar a design as possible to the conventional re-entrant bowl - the bowl volume and hence compression ratio is held constant between the two designs. The stepped lip bowl has a small step around the circumference of the bowl lip with a minor adjustment to the omega part of the bowl to retain the same volume. A relative comparison between the two shapes is shown in Figure 1.

Standard



Stepped



Figure 1: Relative comparison between two bowl shapes tested

Instrumentation

The instrumentation used in this work and their associated uncertainties are detailed in [18], key components are outlined here and in Table 2 for convenience; a schematic of the test facility is shown in Figure 2. The single cylinder engine is not fitted with a turbocharger, rather the inlet air conditions are supplied by an external boosting rig. Cooled, high pressure EGR (driven by pressure difference between the inlet and exhaust) is inserted approximately 1m upstream of a small mixing plenum, ensuring that the EGR is well mixed with the inlet air. Exhaust emissions are measured by a Horiba MEXA-ONE emissions analyser, and an AVL415S smoke meter. In addition to the MEXA unit, an ETAS ES430 compatible lambda sensor was used as a cross-check. The engine is not fitted with a catalyst, nor a DPF, hence the emissions measured are raw engine out emissions, which are sampled approximately 1m downstream from the exhaust back-pressure valve (BPV) at approximately atmospheric pressure.

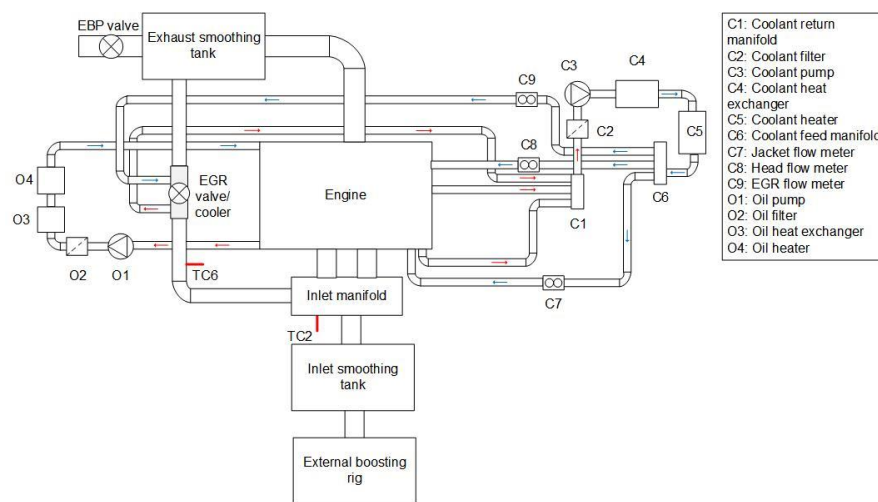


Figure 2: Test cell schematic (adapted from [19])

Table 2: Experimental uncertainties

Oil temperature	$\pm 1\text{ }^{\circ}\text{C}$
Coolant temperature	$\pm 2\text{ }^{\circ}\text{C}$
Inlet air pressure	$\pm 0.5\%$
Inlet air temperature	$\pm 1\text{ }^{\circ}\text{C}$
ISFC	$\pm 1.5\%$
FSN	$\pm 5\%$
Other emissions	0.5 % of full scale

A Pi Innovo M670 OpenECU is used for engine control. This ECU, based on a Jaguar Land Rover built Simulink model, offers full control of the fuel injection equipment, as well as the EGR valve fitted to the engine. Low-speed data is logged at

1 Hz, whereas high speed data acquisition, captured with 0.1 CAD resolution using an AVL IndiSet, is used for four Kistler pressure transducers (cylinder pressure, exhaust pressure, and individual intake port pressures [20]) as well as a current clamp signal indicating fuel injector triggering.

Fuel

A standard (EN590) B0 test diesel was used [21]. The properties of this diesel fuel are shown in Table 3:

Table 3: Diesel composition

Cetane Number	53.0
IBP (°C)	174.1
FBP (°C)	355.0
Aromatics (% m/m)	25.1
Sulfur (mg/kg)	6.5
FAME (% v/v)	< 0.1
Density (kg/L)	0.8327
Lubricity (micron)	322
Viscosity (mm ² /s)	2.783

CFD – model

A commercial CFD code capable of modelling unsteady turbulent combusting flows with moving boundaries was used for all simulations [22]. The computational setup used in this investigation is based on work carried out in [23]; hence, only a brief overview of the models will be given.

The ECFM-3Z model coupled with tabulated kinetic ignition (TKI) was used for combustion modelling [24]. Turbulence closure was accounted for through the well-known RNG-k-epsilon model [25] with heat transfer to the walls being modelled with the Han & Reitz model [26]. The discrete droplet methodology was used to simulate the liquid phase with spray injection and breakup modelled by the Reitz-Diwakar [27] and KH-RT [28] models respectively. Additionally, dynamic droplet drag [29], NTC collisions [30] and the Frossling correlation [31] were used to model droplet drag, collisions and vaporisation.

The computational domain was limited to a 45 degree sector of the engine cylinder only simulating a single nozzle of the equispaced injector. The CFD code generates the grid at runtime using a Cartesian cut cell algorithm with the possibility of using adaptive mesh refinement (AMR) and fixed grid embedding (constant addition of cells in defined volume of the computational domain) to refine regions of interest. In the current work, AMR is based on velocity and temperature gradients with fixed embedding applied a-priori to the near nozzle region during fuel injection. Figure 3 shows the

computational domain and graphically represents the areas that the different grid refinement methodologies are applied as well as cut-plane definitions that will be referred to in later sections of the paper.

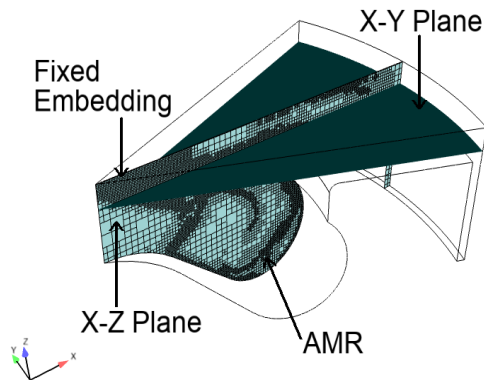


Figure 3: Computational domain showing grid refinement methods and cut-plane definition showing the X-Z plane and X-Y plane and the regions where AMR and fixed grid embedding are applied.

The simulations were run from just after IVC to before EVO. In-cylinder conditions were initialised with experimental pressure measurements, species concentrations from equilibrium balance at the experimental AFR, and the swirl ratio determined from full cycle simulations of the corresponding test point. Wall temperatures were fixed for each simulation and were based on FEA studies. Finally, fuel injection rates for each test point were generated from a 1D dynamic model of the injector.

CFD – emissions models

NO formation was modelled with the Extended Zeldovich Mechanism [32]. This model describes the principle pathways of NO formation: (1) high temperature oxidation of diatomic nitrogen, (2) oxidation of nitrogen from the dissociation of O_2 and (3) NO formation through the combination of N with the hydroxyl radical, OH.

The empirical model of Hiroyasu was used to model soot formation, this was coupled with the Nagle and Strickland-Constable model to simulate soot oxidation [33, 34]. Soot production in the Hiroyasu model is determined from a single step competing reaction between soot oxidation and soot formation rates. These reaction rates are of an Arrhenius type expression and are a function of local thermochemical conditions. A comprehensive description of the model and recommended model constants can be found in [22].

CFD – validation

The CFD model was validated for each test point at a baseline experimental condition – using the re-entrant bowl and 0% EGR. Figure 4 shows the comparison of the cylinder pressure traces and cumulative heat release between experiment and simulation for one part load and one full load test point. It can be seen that the simulation is in good agreement with

experimental data across load points with only some minor differences during the pilot burn and after TDC. These differences result from the uncertainty in the injection rates which were generated from the 1D dynamic model of the injector and common rail system in AMESim (Siemens PLM), as such, accuracy of the final rate shapes is dependent upon the extensiveness of the model and its ability to capture the complex behaviour of high pressure common rail injection systems. There is a slight under-prediction in the final value for the cumulative heat released attributed by the authors to the uncertainty in wall temperatures, which were derived from FEA studies, and the choice of heat transfer model. As in previous studies [18, 22, 23], the authors have found that the heat flux predicted by different heat transfer models can vary significantly. It was consistently found that the lowest heat loss was predicted by the Angelberger model followed by the O'Rourke model with the Han & Reitz model always predicting the greatest heat loss. The Han & Reitz model was chosen for this work as it provided the best match to the experimental data.

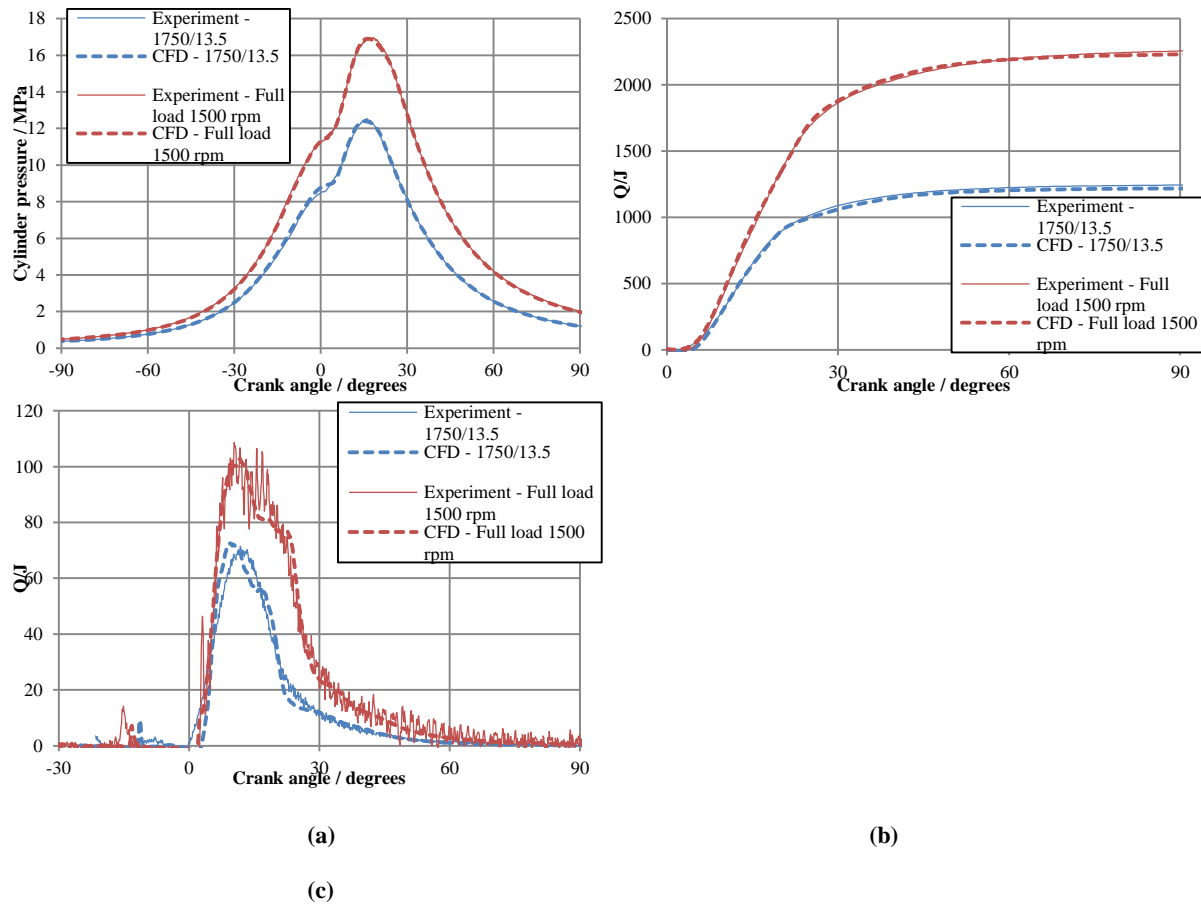


Figure 4: Comparison between experimental and CFD cylinder pressure traces (a), cumulative heat release (b), and instantaneous heat release (c) validating the CFD used.

Test procedure

The engine was run and simulated in CFD at two steady state speed/load operating points, one at a low load (6.8 bar net IMEP) and one at a medium load (13.5 bar net IMEP). At these two part-load conditions, the EGR rate was varied at constant exhaust back-pressure and inlet manifold pressure within the range shown in Table 4. In addition, full load curves were run at four engine speeds at 0 % EGR. The injection timing remained fixed for each test point, with a small pilot of fixed quantity. The engine load was set by varying the main injection quantity to match the desired nIMEP, which was held constant through the EGR sweep. At full load the injection advance was limited by peak cylinder pressure, and the injected fuel quantity was limited by exhaust temperature. The engine operating conditions are shown in Table 4.

Table 4: Engine test conditions

Test point	1500 rpm/6.8 bar nIMEP	1750 rpm/13.5 bar nIMEP	FL1500	FL2000	FL3000	FL4000
Engine speed (rpm)	1500	1750	1500	2000	3000	4000
Net IMEP (bar)	6.8	13.5	Max [†]			
Inlet manifold pressure (barG)	0.25	1.0	1.55	1.85	1.95	1.65
Exhaust back-pressure (barG)	0.45	1.4	1.9	1.75	2.4	2.5
Inlet air temperature (°C)	Varies with EGR		40	45	50	50
Coolant and oil temperature (°C)	90					
EGR levels (approx.)	0-40%	0-27%	0			
Fuel rail pressure (MPa)	55	90	110	145	180	180

[†]Maximum IMEP limited by peak cylinder pressure and maximum exhaust temperature

The “low-speed” data (all data except the injector signal, inlet, exhaust, and in-cylinder pressures) at each test point were measured for three minutes, and a mean was taken. The “high-speed” data were logged at a resolution of 0.1 CAD. Each point was run at least three times, non-sequentially over a number of different days, to ensure repeatability. All emissions and fuel consumption readings have been rescaled by dividing by a nominal value – the same nominal value for all load points but different for each parameter (e.g. ISFC, ISNO_x etc.) and chosen to ensure the maximum values of the data presented is close to 1. All of the data is presented against ISNO_x, acting as an indicator of the external EGR levels with values closest to 1 indicating no EGR, and values closest to 0 indicating the maximum level of EGR tested.

Results and discussion

Part load

The experimental part load results from this work have been reported in a previous publication by the authors [18]. It was noted that the stepped lip bowl increased 50-90 % MFB durations by approximately 3 degrees crank angle compared to the re-entrant bowl for all EGR levels. This was noted to be in direct contrast to the existing literature pertaining to stepped bowl pistons [4, 9] and was attributed to flame ‘hold-up’ in the step region of the bowl. In the current study, we will use new multi-dimensional simulations to help understand and explain the combustion and emissions trends observed in [11] and we will extend the research to include full load operation.

Figures 5 and 6 show the NO_x -Soot emissions across the EGR range for both bowls at the two part load test points. There is generally good agreement between experimental and numerical results with the experimental emissions trends, a minor increase in NO_x and decrease in soot with the stepped bowl, correctly captured by the simulations at the 1750 rpm/13.5 bar nIMEP condition (Figure 6) – a detail which is not captured by the CFD emissions models at the 1500 rpm/6.8 bar nIMEP operating condition (Figure 5). We note however that the differences in soot emissions between the two bowl designs are often within one standard deviation and that therefore, although the trends are consistent, the results have limited statistical certainty. Note also that the observed deviations between the experimental and simulation results can be attributed in-part to variations of experimental EGR rate away from the nominal target value and, as will be discussed later, fundamental differences in measurement location.

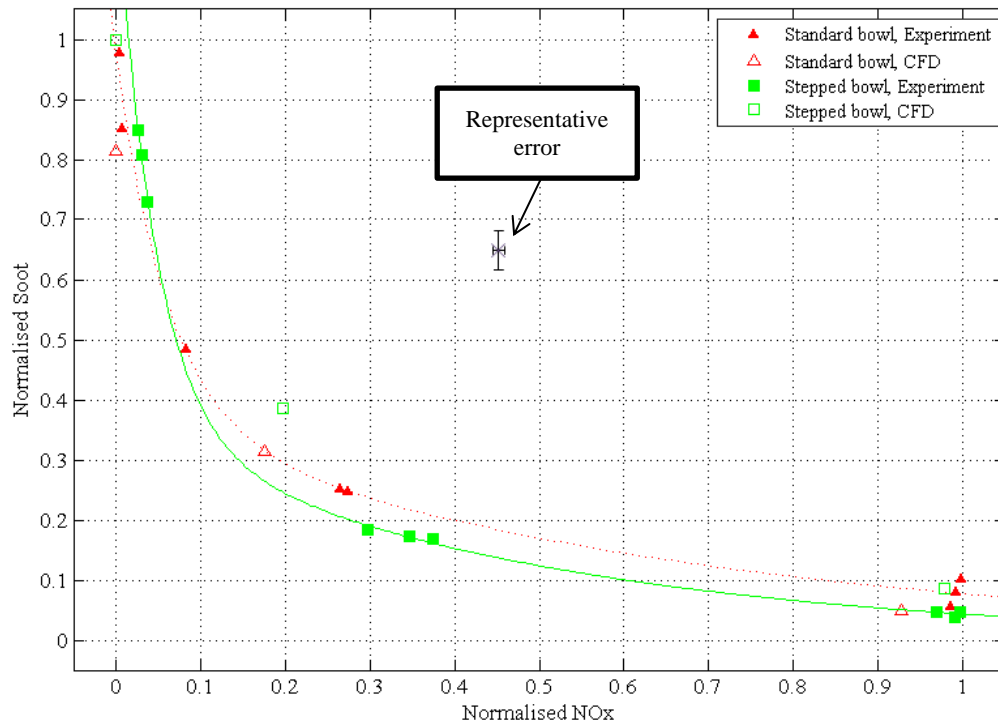


Figure 5: Normalised NO_x-soot tradeoff at 1500 rpm/6.8 bar nIMEP showing both experimental results and the prediction from CFD (experimental NO_x in ppm, CFD NO_x in kg, and experimental soot in FSN, CFD soot in kg). For clarity, a representative error of $\pm\sigma$ for the experimental data is shown

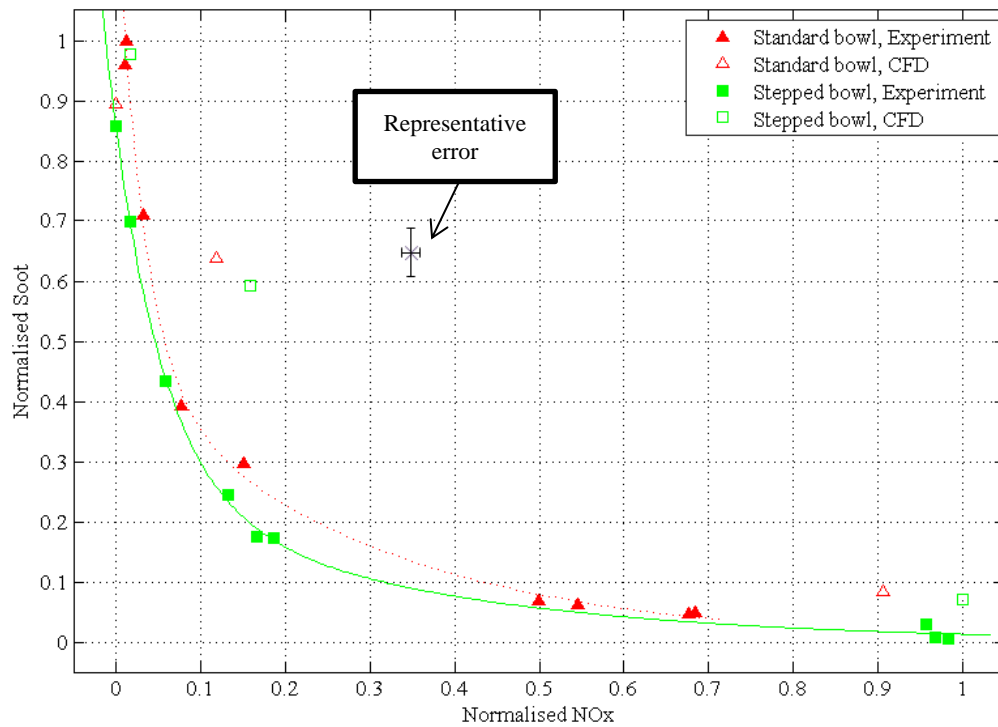


Figure 6: Normalised NO_x-soot tradeoff at 1750 rpm/13.5 bar nIMEP showing both experimental results and the prediction from CFD (experimental NO_x in ppm, CFD NO_x in kg, and experimental soot in FSN, CFD soot in kg). For clarity, a representative error for the experimental data of $\pm\sigma$ is shown

The CFD predictions of in-cylinder temperature and equivalence ratio (ϕ) at 1750 rpm/13.5 bar nIMEP (Figure 7) help explain the experimentally observed emissions results. The combustion event can be seen to penetrate further into the high temperature region around $\phi=1$ with the stepped lip piston than with the standard re-entrant bowl; this area is where the greatest amount of NO_x is formed [32]. These higher in-cylinder temperatures (particularly at 50 CAD atdc) will also increase soot oxidation (i.e. cause a reduction in soot). CFD results suggest that the increased in-cylinder temperature with the stepped bowl design is likely due to changes in the spatial equivalence ratio distribution. Figure 8 shows that there is less fuel in the squish region of the cylinder and hence more fuel within the bowl for the stepped piston design.

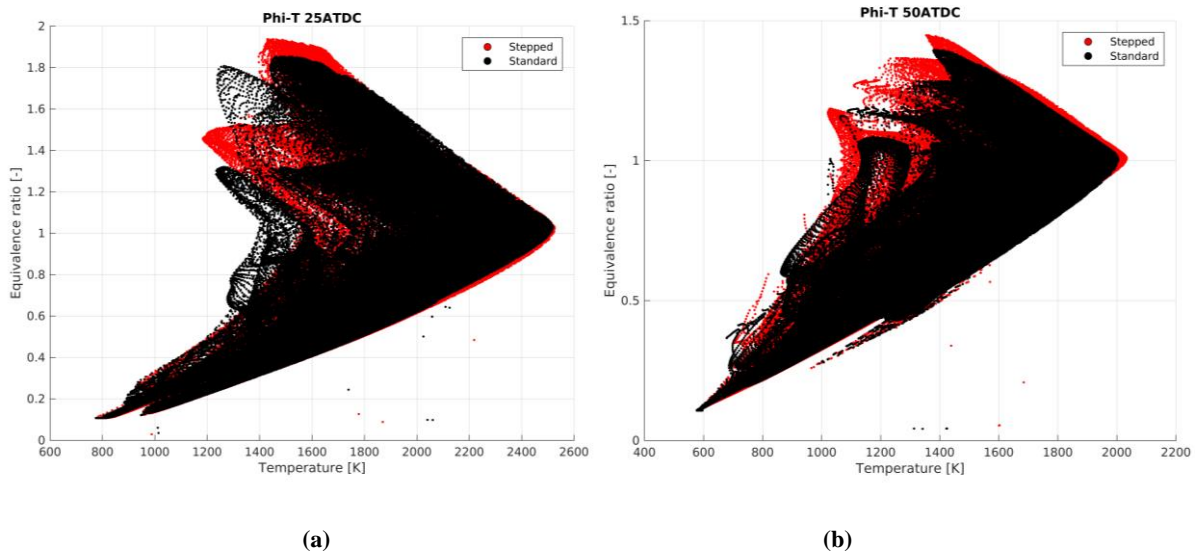


Figure 7: CFD predictions of local in-cylinder temperature and equivalence ratio (ϕ) at 1750 rpm/13.5 bar nIMEP at 25 (a) and 50 (b) CAD atdc at a normalized NO_x of ~ 0.15 .

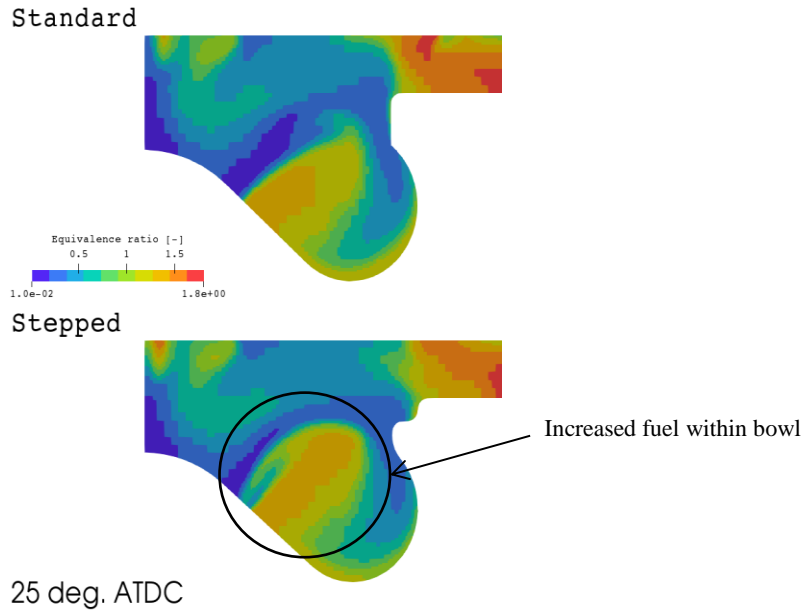


Figure 8: Predicted in-cylinder equivalence ratio (ϕ) for the standard bowl (upper) and stepped (lower) at 1750 rpm/13.5 bar nIMEP at a normalized NO_x of ~ 0.15 .

Full load results

The full load operating points were run at four engine speeds (1500, 2000, 3000, and 4000 rpm). Note that full load operating points in this work are defined as being the operating points of maximum possible fuel injection advance and maximum injected fuel quantity within the limits imposed by a specified maximum cylinder pressure and exhaust temperature. The engine operating parameters were shown in Table 4. CFD simulations were only conducted at (1500, 2000, and 4000 rpm) due to run-time constraints. The experimental results show the results from one full load curve.

Figure 9 shows the measured smoke emissions (FSN) and predicted soot mass from the engine at full load. The experimental results (Figure 9a) suggest that there may be minor reductions in soot emissions associated with the stepped lip design; however the results are not statistically significant within the current data set. In contrast, the CFD predictions of soot mass shown in Figure 9b suggest that the stepped lip design may very slightly increase soot emissions at the 1500 and 2000 rpm operating points. A significant increase in soot emissions is also predicted as the engine speed is increased from 2000 rpm to 4000 rpm whereas the experimental results show a decrease with respect to the 2000 and 3000 rpm engine speeds. These results clearly demonstrate the challenges of making direct comparisons between the experimental and numerical soot data; the CFD model predicts the soot mass in cylinder as the exhaust valve opens, whereas the experimental results are measured some way downstream of the exhaust valve using a smoke meter, which measures the opacity of a soot sample collected on a filter paper. In practice, there will be significant post flame oxidation at 4000 rpm due to exhaust temperatures over 810°C that is not accounted for in the CFD model and thus the relative over-prediction of the soot at this condition is to be expected (this is true at 3000 rpm as well, but this case is not modelled in CFD).

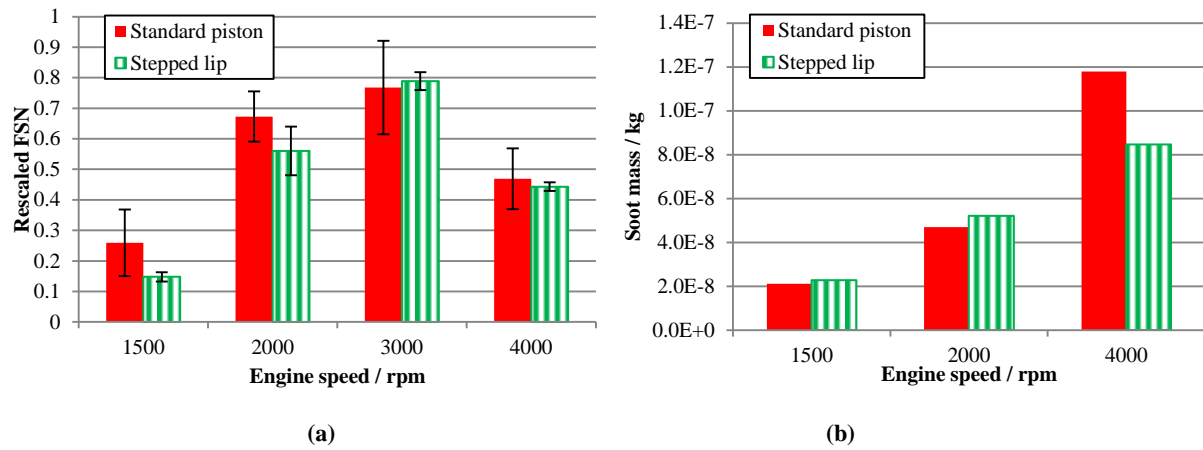


Figure 9: Measured FSN emissions (a) and CFD predicted soot mass (b) from the engine at full load. Error bars correspond to $\pm\sigma$.

Figure 10 shows the measured ISNO_x emissions from the engine at full load and the corresponding NO_x mass predictions from the CFD model. Since NO_x is measured more directly than soot, the experimental data can be compared more directly with the predicted NO_x emissions. Small, but statistically significant (~67 % Confidence Interval (CI)), increases in ISNO_x emissions are observed experimentally with the stepped lip piston at the 2000 and 4000 rpm test points. The trends shown in the experimental results are closely matched by the CFD at 1500 rpm and 4000 rpm – with the stepped lip piston showing an increase in NO_x at 4000 rpm. However, the model does not predict the NO_x increase observed in the experiments at 2000 rpm.

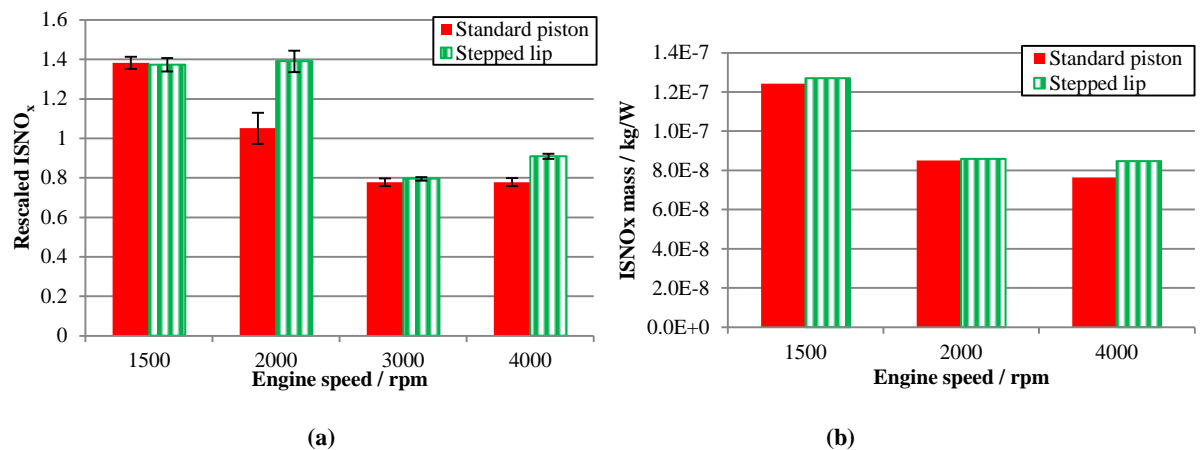


Figure 10: Measured ISNO_x emissions (a) and CFD predicted NO_x mass (b) from the engine at full load. The error bars correspond to $\pm\sigma$.

The in-cylinder CFD gives a good insight as to why NO_x emissions are increased at 4000 rpm with the stepped lip design.

The model predicts an increase in in-cylinder flame temperature (Figure 11) in the area around where the fuel spray is being

injected (top left of the images), particularly at around the time when the fuel injection is ending (25-35 CAD). This is predicted to result in significantly higher local NO_x formation (Figure 12). Higher temperatures are seen in the fire-land with the stepped lip bowl that, while helpful for soot oxidation, will also contribute to higher thermal NO_x formation.

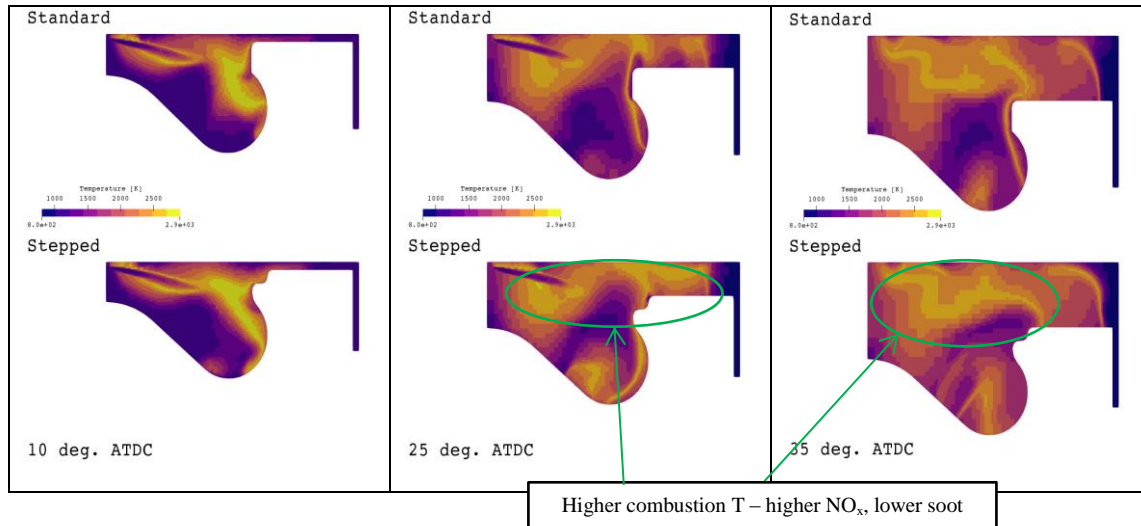


Figure 11: Predicted in-cylinder temperature at three crank angles for both the standard bowl (upper) and stepped lip bowl (lower) at 4000 rpm. The areas of high temperature are consistent with areas of higher NO_x formation shown in Figure 10.

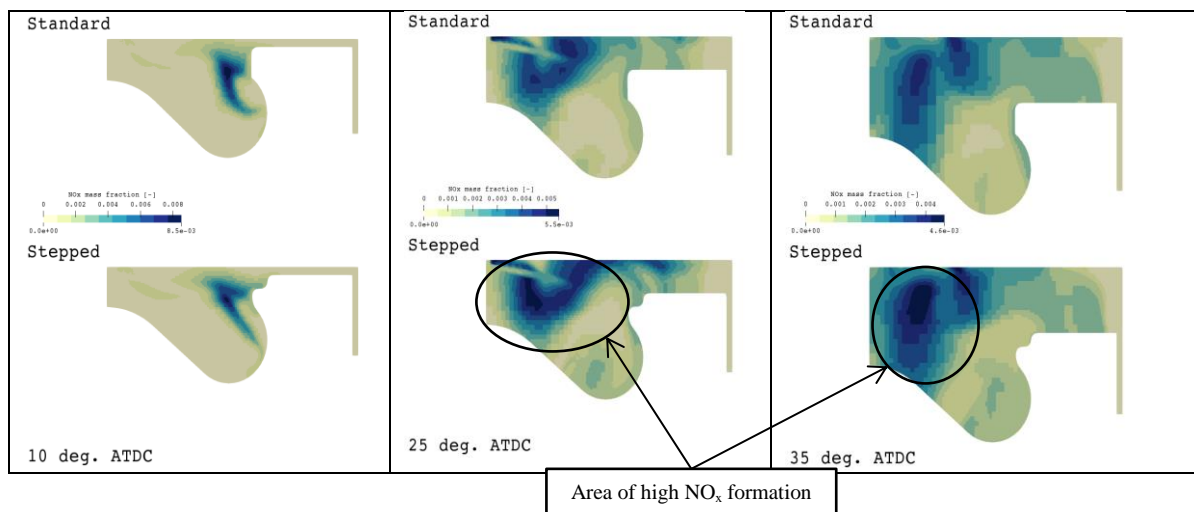


Figure 12: Predicted in-cylinder NO_x mass fraction at three crank angles for both the standard bowl (upper) and stepped lip bowl (lower) at 4000 rpm, full load. Areas of high NO_x formation are noted consistent with higher combustion temperatures shown in Figure 11.

Figure 13 shows the ISFC across the full load curve. In general there is little difference with bowl shape at lower engine speeds, however at higher engine speeds the stepped lip piston shows a marginally lower ISFC compared to the standard bowl (statistically significant at 67% CI). The authors' hypothesis for this reduction, presented below, draws from the results of both the present study and a related Nozzle Tip Protrusion (NTP) study, which will be reported separately, so as to add statistical value.

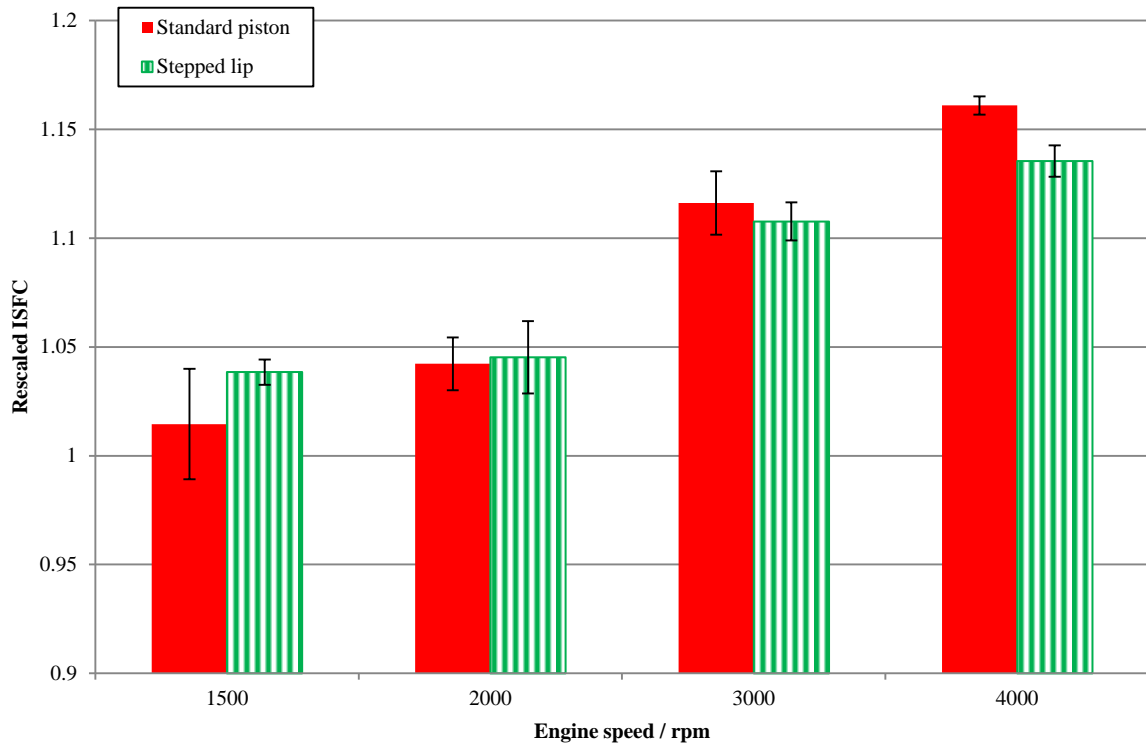


Figure 13: Measured full load ISFC. Very little difference between pistons is observed. The error bars correspond to $\pm\sigma$.

Firstly, it is important to note that full load in this study is a highly constrained operating condition defined as the maximum fuel injection advance possible while remaining below the maximum cylinder pressure sustainable and with the maximum fuel quantity injected while remaining below the maximum exhaust temperature permitted. The maximum fuel injection advance achieved within the stated limits at each point is shown Table 5 (here NTP 1 and NTP 2 differ by 0.5 mm). The exhaust temperatures and peak firing pressures are shown in Figures 14 and 15. Inevitably operating the engine in this region over the three minute logging duration will lead to some natural variations in the maximum cylinder pressure and exhaust temperature that must be considered, given the definition of full load, in order to ensure that any comparisons drawn are valid. It can be seen that at 1500 and 2000 rpm there are statistically significant (~67 % CI) increases in exhaust temperature, and similarly significantly increases in peak firing pressure at 1500 and 3000 rpm that add an acknowledged degree of uncertainty to our results.

Table 5: Stepped lip bowl ignition advance with respect to standard re-entrant bowl at full load.

Engine Speed (rpm)	Nozzle tip protrusion	Ignition advance ($^{\circ}\text{CA}$)
1500	NTP 1	0.7
	NTP 2	0.7
2000	NTP 1	0.0
	NTP 2	0.0

3000	NTP 1	0.7
	NTP 2	1.2
4000	NTP 1	1.0
	NTP 2	1.8

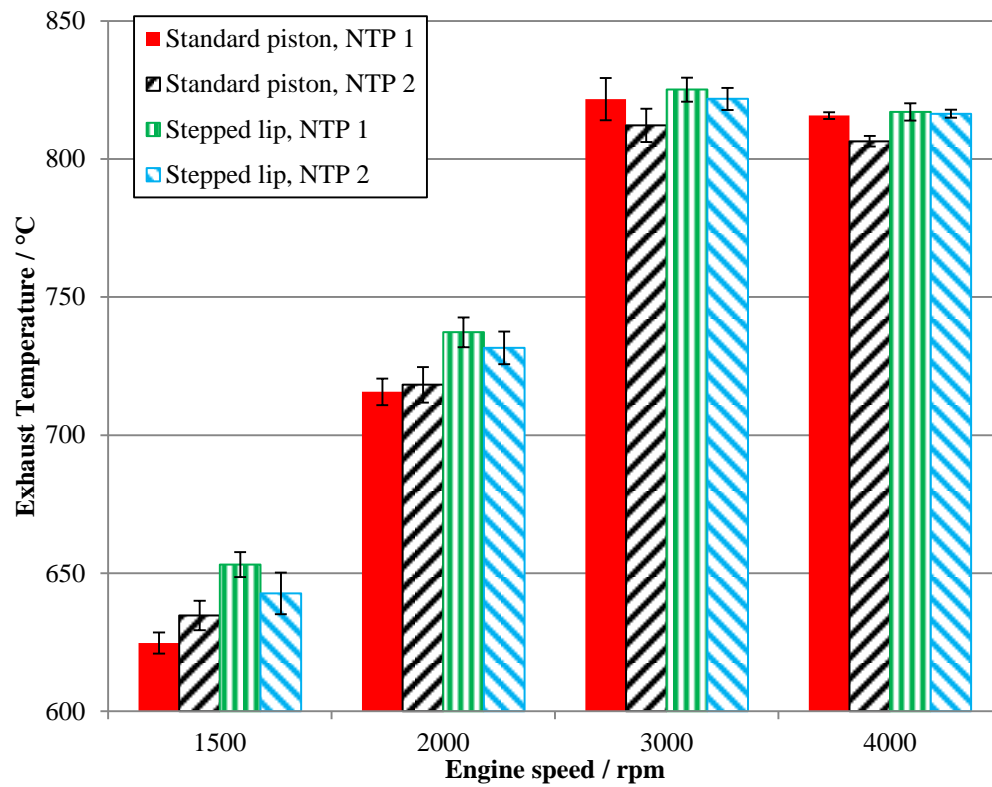


Figure 14: Measured exhaust temperature during the full load curve. The error bars correspond to $\pm\sigma$.

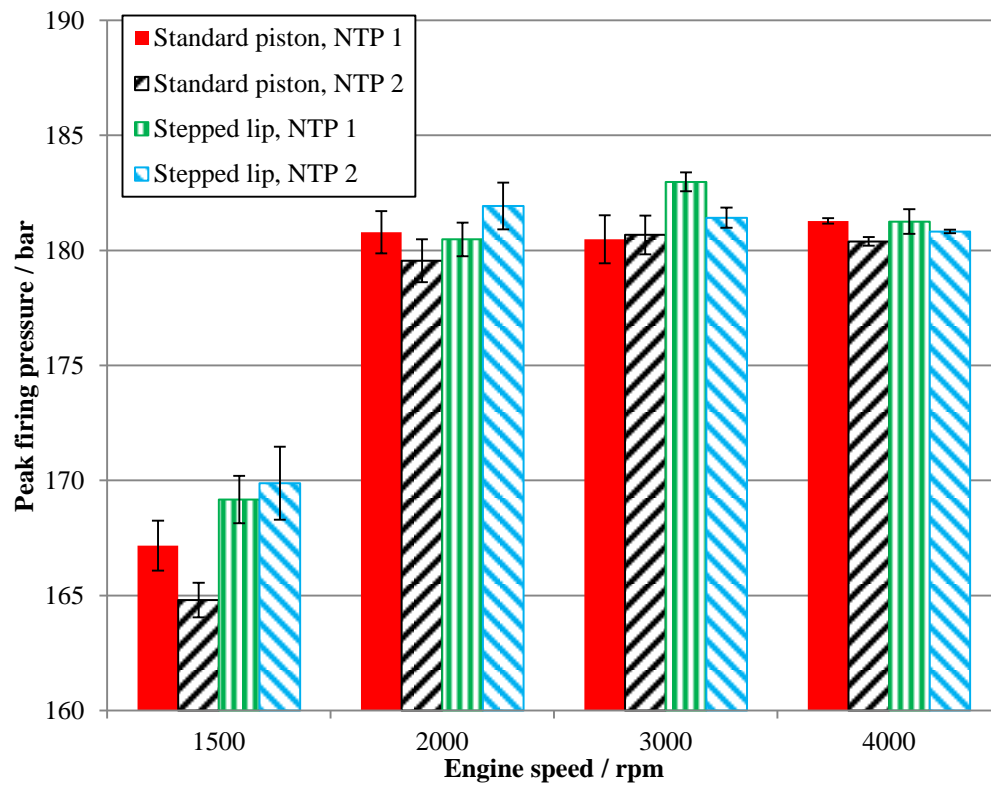


Figure 15: Measured peak firing pressure during the full load curve. The error bars correspond to $\pm\sigma$.

Figure 16 shows the measured full load nIMEPs. The results show that at all engine speeds, the stepped piston gave a higher nIMEP than the re-entrant bowl piston design (although at higher engine speeds the effect is less pronounced). At 1500 and 2000 rpm this could be attributed to the observed increases in exhaust temperatures and peak firing pressures (these parameters are restrictions on the maximum nIMEP achievable), however at 3000 and 4000 rpm Figures 14 and 15 show the exhaust temperatures and peak pressures for a given NTP to be constant within the limits of statistical certainty suggesting that the observed increase in nIMEP at these engine speeds may be attributed to the variation of the bowl shape. Specifically, the authors suggest that the observed increases in nIMEP with the stepped lip piston at the higher engine speeds is the direct result of the more advanced injection timing that was achievable compared to the standard piston whilst remaining within allowable exhaust temperature and cylinder pressure limits (Table 5).

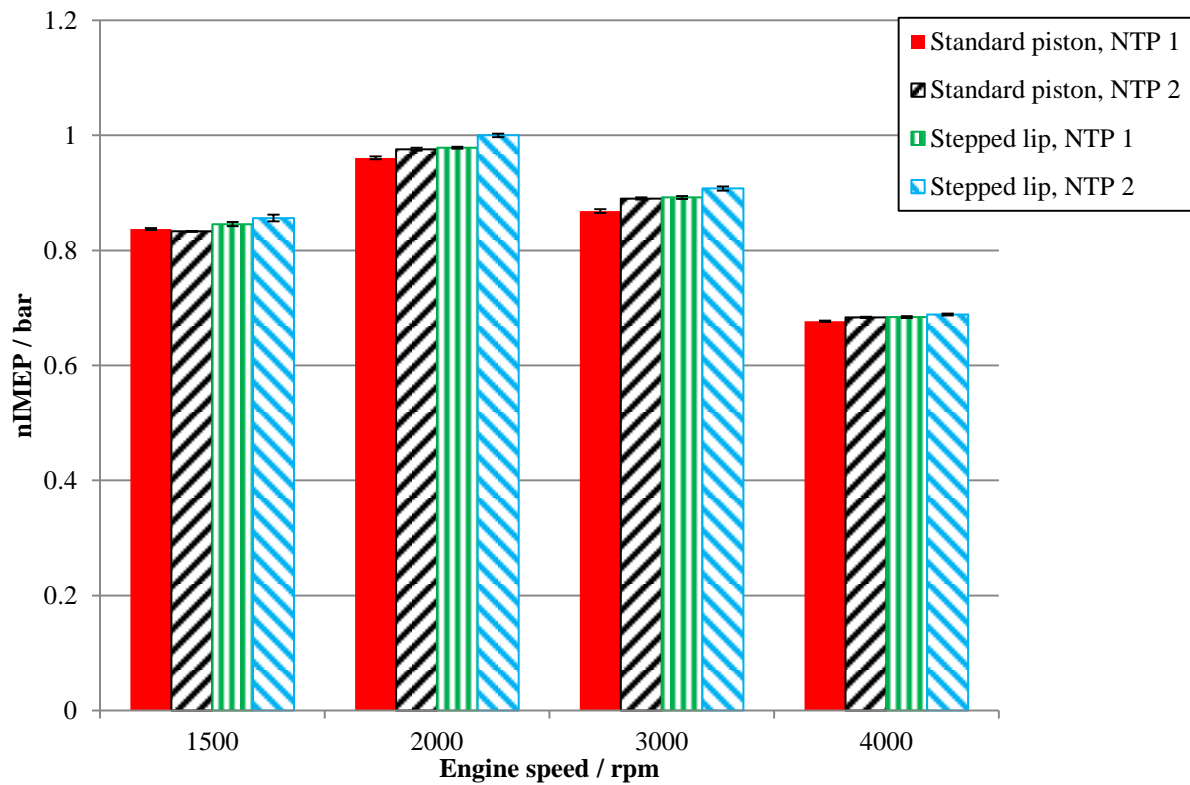


Figure 16: nIMEPs achieved at full load at four engine speeds; an increase in peak power can be seen for the stepped piston at all engine speeds. The error bars correspond to $\pm\sigma$.

Figure 17 shows the 10-50 % and 50-90 % mass fraction burn (MFB) durations for the engine at full load. A minor increase in the 10-50 % MFB durations across the full load curve is observed with the stepped lip piston; the stepped lip piston gives significantly longer 50-90 % MFB durations, in line with the results reported in the literature at part load [23]. Particularly at 4000 rpm this increase in 50-90 % MFB duration may explain why a greater injection timing advance is possible with the stepped lip bowl (Table 5), as the cylinder pressure rise rate will be slower, allowing a greater injection advance before reaching the maximum cylinder pressure. Numerical simulations give strong insight into the cause of the increased combustion duration with the stepped bowl.

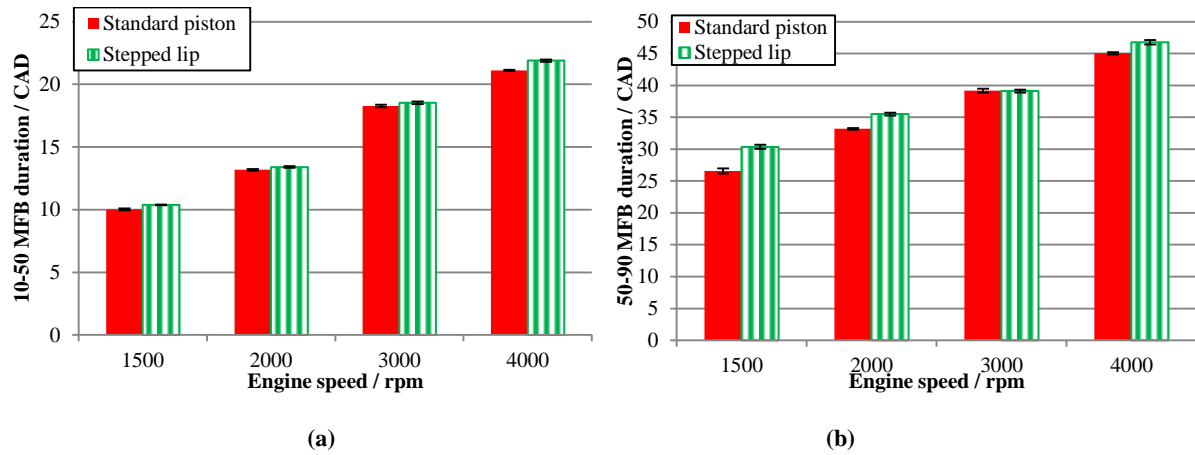


Figure 17a: 10-50 % (a) and 50-90 % (b) MFB duration measured across the full load curve. The error bars correspond to $\pm\sigma$.

Figure 18 shows the predicted in-cylinder temperature at 10, 15, and 20 ° ATDC with the standard and stepped lip pistons at full load, 1500 rpm. The stepped lip is seen to slow down or trap the flame in the lip region, preventing the rapid movement of the flame across the fire-land. This behavior is consistent with the authors' observation of combustion behavior with the stepped lip bowl at part-load [11]. Figure 19, which shows the predicted in-cylinder velocities, adds more detail. The lip feature causes the velocities to reduce to almost zero at 10 ° ATDC which subsequently develops into a recirculation at later crank angles – flow features not seen with the standard piston – thus explaining the mechanism of the flame ‘hold-up’ at the lip. The predicted flame ‘hold-up’ phenomenon explains not only why the MFB durations are increased for the stepped lip piston (Figure 17) but also why the ignition may be advanced further with the stepped lip piston. Since it is known that more advanced injection timings can decrease ISFC [35] this may then explain the observed decrease in ISFC at higher engine speeds for the stepped lip piston.

The decrease in burn rate that we have observed both experimentally and numerically in this work contrasts sharply with the published literature [7, 11, 12] where, consistently, stepped lip pistons have been shown to increase burn rate. We note however that the pistons studied in the referenced works have had a more ramped shape to the bowl lip as distinct from the definite step feature of the piston in the current study. To the authors' knowledge, the decrease in burn rate seen in the current work has not been reported in the open literature for full load operation. The results presented here, which are necessarily preliminary in nature due to the limited number of data points available, suggest that the stepped bowl design may have potential advantages at the full load points including higher achievable maximum powers and a potential decreases in ISFC at higher engine speeds. Further, detailed studies are required to confirm this potential with higher statistical certainty.

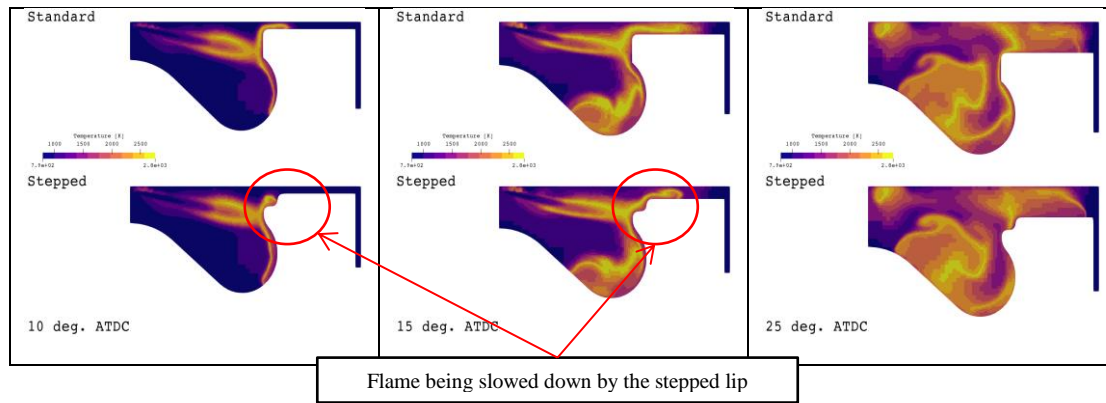


Figure 18: Predicted in-cylinder temperature at three crank angles for both the standard bowl (upper) and stepped lip bowl (lower) at full load, 1500 rpm at 10, 15, and 25 ° ATDC.

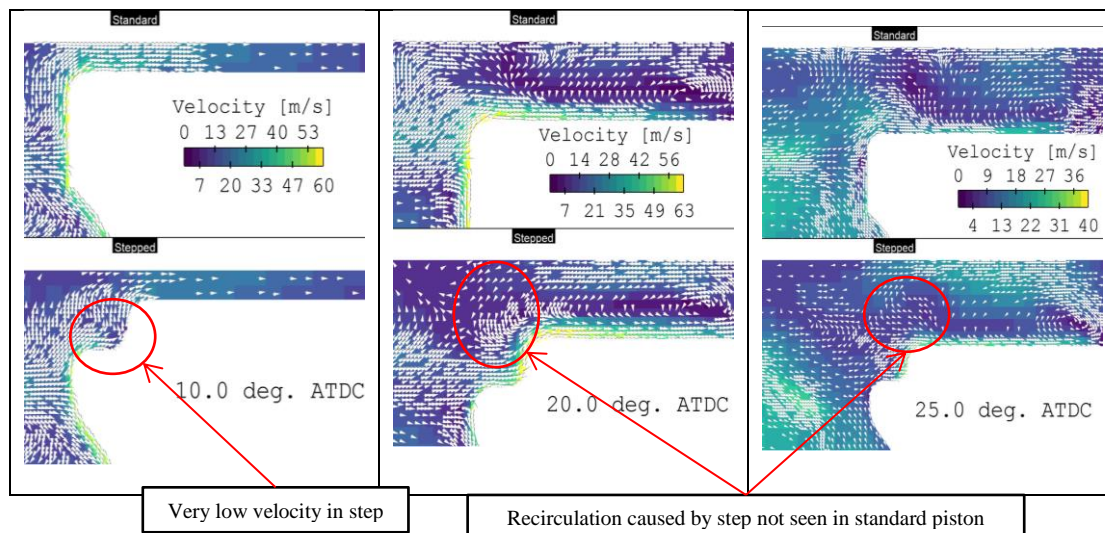


Figure 19: Predicted in-cylinder velocities at three crank angles for both the standard bowl (upper) and stepped lip bowl (lower) at full load, 1500 rpm at 10, 20, and 25 ° ATDC.

Conclusions

This study considers the effects of two piston bowl shapes, a conventional re-entrant bowl and a 'stepped' lip bowl, on combustion and emissions from a light-duty high-speed diesel engine at two part-load operating points (1500 rpm/6.8 bar net IMEP and 1750 rpm/13.5 bar net IMEP), and four full-load operating points (1500, 2000, 3000, and 4000 rpm). Multi-dimensional CFD modelling is used to provide insight into the details of the spray, mixing, and combustion processes at each operating point and to explain the experimentally observed combustion and emissions trends. The results show that:

- Burn rates, and in particular the 50-90% MFB rate, are slower at all operating speeds and loads for the stepped lip bowl design compared to the standard re-entrant bowl. This slower burn rate is contrary to previously reported results for stepped bowls.

- The reduction in burn rates with the stepped lip bowl design is due to changes in the flow field local to the piston ‘step’. The very low flow velocities found in the step region shortly after TDC lead to a recirculation zone at the bowl lip that is not seen with the standard piston. This recirculation zone effectively slows down or traps the flame in the lip region.
- The stepped lip bowl design permits a small (~ 1 CAD) advance in main fuel injection timing compared with the standard re-entrant bowl at full load; a condition constrained in this work by defined limits of cylinder pressure and exhaust temperature.
- It may be possible to exploit the flame ‘hold-up’ effect associated with the stepped lip piston design to achieve higher engine power at full load, although we note that exhaust temperatures and peak pressures were not perfectly controlled in the present work and that further investigation would be required to confirm or refute this conclusion.
- There is no statistical difference in NO_x and soot emissions between the two bowl geometries at part load. The part-load NO_x /Soot curves for the stepped lip bowl design are consistently within one standard deviation of the results from the standard re-entrant bowl.
- There is a minor penalty in NO_x emissions (statistically significant at (~ 67 % CI) associated with the stepped lip bowl at some full load points.
- Comparisons between experimental and predicted soot are particularly challenging at full load due to the substantial levels of post-flame oxidation associated with the high temperature exhaust gas.

Overall, there was no significant change in other engine parameters such as ISFC observed with the stepped lip piston.

Further work will investigate the thermal advantages of this type of stepped lip design, noting that the stepped lip is closer to the piston cooling gallery than the equivalent lip on the standard piston. This might have important advantages for production vehicles using this design of piston.

Acknowledgements

The authors would like to thank Jaguar Land Rover Limited and Oxford University Press John Fell fund for financial support. The authors would also like to thank BP International for supplying the diesel fuel. The authors would like to thank Liyah Dholiwar for undertaking much of the engine testing and the Department of Engineering Science technicians and maintenance teams for facilities support.

References

1. Stone, R., *Introduction to internal combustion engines*. 2012: Palgrave Macmillan.
2. ICCT, *Estimated Cost of Emission Reduction Technologies for Light-Duty Vehicles*. 2012.

3. Kook, S., et al., *The Effect of Swirl Ratio and Fuel Injection Parameters on CO Emission and Fuel Conversion Efficiency for High-Dilution, Low-Temperature Combustion in an Automotive Diesel Engine*. SAE Technical Paper 2006-01-0197, 2006.
4. Dakhore, R., et al., *Effect of Piston Cavity Geometry on Combustion, Emission and Performance of a Medium Duty DI Diesel Engine*. SAE Technical Paper 2015-26-0198, 2015.
5. Yu, H., et al., *Numerical investigation of the effect of two-stage injection strategy on combustion and emission characteristics of a diesel engine*. Applied Energy, 2017.
6. d'Ambrosio, S. and A. Ferrari, *Diesel engines equipped with piezoelectric and solenoid injectors: hydraulic performance of the injectors and comparison of the emissions, noise and fuel consumption*. Applied Energy, 2018. **211**: p. 1324-1342.
7. Dahlstrom, J., et al., *Experimental Comparison of Heat Losses in Stepped-Bowl and Re-Entrant Combustion Chambers in a Light Duty Diesel Engine*. SAE Technical Paper 2016-01-0732, 2016.
8. Fridriksson, H., et al., *Effect of Piston Bowl Shape and Swirl Ratio on Engine Heat Transfer in a Light-Duty Diesel Engine*. SAE Technical Paper 2014-01-1141, 2014.
9. Lee, J., et al., *Bowl Shape Design Optimization for Engine-Out PM Reduction in Heavy Duty Diesel Engine*. 2015, SAE Technical Paper.
10. Nishida, K., et al., *Small Bore Diesel Engine Combustion Concept*. 2015, SAE Technical Paper.
11. Dolak, J.G., Y. Shi, and R.D. Reitz, *A computational investigation of stepped-bowl piston geometry for a light duty engine operating at low load*. 2010, SAE Technical Paper.
12. Busch, S., F. Perini, and R.D. Reitz, *Light-Duty Diesel Combustion*, C.R.F. Sandia National Laboratories, Editor. 2016.
13. Federico, P., et al., *Piston geometry effects in a light-duty, swirl-supported diesel engine: Flow structure characterization*. International Journal of Engine Research, 2017: p. 1468087417742572.
14. Miles, P.C. and Ö. Andersson, *A review of design considerations for light-duty diesel combustion systems*. International Journal of Engine Research, 2015. **17**(1): p. 6-15.
15. Lückert, P., et al. *The New Mercedes-Benz 4-Cylinder Diesel Engine OM 654—The Innovative Base Engine Of The New Diesel Generation*. in *24th Aachen Colloquium Automobile and Engine Technology*. 2015.
16. Eder, T., et al., *OM 654—Launch of a New Engine Family by Mercedes-Benz*. MTZ worldwide, 2016. **77**(3): p. 60-67.
17. Chittick, S., M. Swindell, and S. Raorane, *Analytical and Developmental Techniques Utilized in the Structural Optimization of a New Lightweight Diesel Engine*. SAE International Journal of Engines, 2015. **8**(4): p. 1960-1966.
18. Leach, F., et al., *Comparing the Effect of Fuel/Air Interactions in a Modern High-Speed Light-Duty Diesel Engine*. SAE Technical Paper, 2017. **2017-24-0075**.
19. Papaioannou, N., et al., *Evaluation of EGR techniques on a HSDI diesel engine using first law analysis*. Proceedings of the Institution of Mechanical Engineers, Part D: Journal of Automobile Engineering, 2018.
20. Leach, F., et al., *Comparing the effect of a swirl flap and asymmetric inlet valve opening on a light duty diesel engine*. SAE Technical Paper, 2017. **2017-01-2429**.
21. EN590, B., *British Standards BS EN 590 Diesel, Requirements and Test Methods*. 2009.
22. Richards, K.J., P.K. Senecal, and E. Pomraning, *CONVERGE (v2.3)*. Convergent Science, 2016.
23. Ismail, R., et al., *Computational Investigation of the Effects of Piston Geometry on the Combustion Evolution in a Light Duty HSDI Engine*, in *ASME 2017 Internal Combustion Fall Technical Conference*. 2017, ASME: Seattle, WA, USA.
24. Colin, O. and A. Benkenida, *The 3-zones extended coherent flame model (ECFM3Z) for computing premixed/diffusion combustion*. Oil & Gas Science and Technology, 2004. **59**(6): p. 593-609.
25. Orszag, S.A., et al., *Renormalization group modeling and turbulence simulations*. Near-wall turbulent flows, 1993: p. 1031-1046.
26. Han, Z. and R.D. Reitz, *A temperature wall function formulation for variable-density turbulent flows with application to engine convective heat transfer modeling*. International Journal of Heat and Mass Transfer, 1997. **40**(3): p. 613-625.
27. Reitz, R.D. and R. Diwakar, *Structure of high-pressure fuel sprays*. 1987, SAE Technical Paper.
28. Reitz, R.D. and F. Bracco, *Mechanisms of breakup of round liquid jets*. Encyclopedia of fluid mechanics, 1986. **3**: p. 233-249.
29. O'Rourke, P.J. and A.A. Amsden, *The TAB method for numerical calculation of spray droplet breakup*. 1987, Los Alamos National Lab., NM (USA).
30. Schmidt, D.P. and C.J. Rutland, *A New Droplet Collision Algorithm*. Journal of Computational Physics, 2000. **164**(1): p. 62-80.
31. Amsden, A.A., P.J. O'Rourke, and T.D. Butler, *KIVA-II: A computer program for chemically reactive flows with sprays*, in *Other Information: Portions of this document are illegible in microfiche products*. 1989. p. Medium: X; Size: Pages: 164.
32. Heywood, J.B., *Internal combustion engine fundamentals*. Vol. 930. 1988: McGraw-hill New York.
33. Hiroyasu, H. and T. Kadota, *Models for Combustion and Formation of Nitric Oxide and Soot in Direct Injection Diesel Engines*. SAE Technical Paper 760129, 1976.
34. Nagle, J. and R. Strickland-Constable. *Oxidation of Carbon between 1000-2000 C*. in *Proceedings of the fifth carbon conference*. 1962. Pergamon Press London.
35. Patterson, D.J. and N.A. Henein, *Emissions from combustion engines and their control*. 1981.

Definitions and abbreviations

AMR	Adaptive Mesh Refinement
CA b(a)TDC	Crank Angle before (after) Top Dead Centre
CA10	Angle of 10% mass fraction burned
CA50	Angle of 50% mass fraction burned
CA90	Angle of 90% mass fraction burned
CAD	Crank Angle Degrees
CFD	Computational Fluid Dynamics
CI	Confidence Interval
EGR	Exhaust Gas Recirculation
FEA	Finite Element Analysis
IMEP	Indicated Mean Effective Pressure
ISFC	Indicated Specific Fuel Consumption
MFB	Mass Fraction Burned
nIMEP	Net Indicated Mean Effective Pressure
NO_x	Nitrogen oxides
NTP	Nozzle Tip Protrusion
Q	Heat energy released
TDC	Top Dead Centre
TKI	Tabulated Kinetic Injection